Variation in RBE for Survival of V79-4 Cells as a Function of Alpha-Particle (Helium Ion) Energy

Authors: Tracy, Bliss L., Stevens, David L., Goodhead, Dudley T., and Hill, Mark A.

Source: Radiation Research, 184(1) : 33-45

Published By: Radiation Research Society

URL: https://doi.org/10.1667/RR13835.1

RADIATION RESEARCH **184**, 33–45 (2015)
0033-7587/15 $15.00

DOI: 10.1667/RR13835.1

Variation in RBE for Survival of V79-4 Cells as a Function of Alpha-Particle (Helium Ion) Energy

Bliss L. Tracy,[a,b] David L. Stevens,[a,c] Dudley T. Goodhead[a] and Mark A. Hill[a,c,1]

[a] *Medical Research Council, Harwell, Oxfordshire OX11 0RD, United Kingdom;* [b] *Radiation Protection Bureau, Health Canada 6302D1, Ottawa, Ontario K1A 1C1, Canada; and* [c] *Cancer Research UK and Medical Research Council Oxford Institute for Radiation Oncology, Gray Laboratories, University of Oxford, Oxford OX3 7DQ, United Kingdom*

Tracy, B. L., Stevens, D. L., Goodhead, D. T. and Hill, M. A. Variation in RBE for Survival of V79-4 Cells as a Function of Alpha-Particle (Helium Ion) Energy. *Radiat. Res.* 184, 33–45 (2015).

High linear energy transfer (LET) α particles are important with respect to the carcinogenic risk associated with human exposure to ionizing radiation, most notably to radon and its progeny. Additionally, the potential use of alpha-particle-emitting radionuclides in radiotherapy is increasingly being explored. Within the body the emitted alpha particles slow down, traversing a number of cells with a range of energies and therefore with varying efficiencies at inducing biological response. The LET of the particle typically rises from between ~70–90 keV μm^{-1} at the start of the track (depending on initial energy) to a peak of ~237 keV μm^{-1} towards the end of the track, before falling again at the very end of its range. To investigate the variation in biological response with incident energy, a plutonium-238 alpha-particle irradiator was calibrated to enable studies with incident energies ranging from 4.0 MeV down to 1.1 MeV. The variation in clonogenic survival of V79-4 cells was determined as a function of incident energy, along with the relative variation in the initial yields of DNA double-strand breaks (DSB) measured using the FAR assay. The clonogenic survival data also extends previously published data obtained at the Medical Research Council (MRC), Harwell using the same cells irradiated with helium ions, with energies ranging from 34.9 MeV to 5.85 MeV. These studies were performed in conjunction with cell morphology measurements on live cells enabling the determination of absorbed dose and calculation of the average LET in the cell. The results show an increase in relative biological effectiveness (RBE) for cell inactivation with decreasing helium ion energy (increasing LET), reaching a maximum for incident energies of ~3.2 MeV and corresponding average LET of 131 keV μm^{-1}, above which the RBE is observed to fall at lower energies (higher LETs). The effectiveness of single alpha-particle traversals (relevant to low-dose exposure) at inducing cell inactivation was observed to increase with decreasing energy to a peak of ~68% survival probability for incident energies of ~1.8 MeV (average LET of 190 keV μm^{-1}) producing ~0.39 lethal lesions per track. However, the efficiency of a single traversal will also vary significantly with cell morphology and angle of incidence, as well as cell type.

INTRODUCTION

The efficiency of ionizing radiation in producing a range of biological effects depends not only on absorbed dose but also on radiation quality and its associated track structure, with biological effectiveness per unit absorbed dose typically increasing with increasing linear energy transfer (LET). High-LET alpha particles are particularly important with respect to human exposures, most notably from radon and its progeny, which contribute approximately 50% of the annual effective dose to the UK population and with a similar contribution worldwide. The effective dose to individuals from radon and its progeny can vary by many orders of magnitude depending on location (*1*). The main decay chain for ^{222}Rn produces α particles ranging in energy from 5.3–7.7 MeV with corresponding ranges in tissue (assumed here to be water) of approximately 40 and 71 μm, respectively. As an alpha particle slows down and loses energy, the LET of the particle rises from between ~70–90 keV μm^{-1} at the start of the track (depending on initial energy) to a peak of ~ 237 keV μm^{-1} at an energy of 0.65 MeV towards the end of the track before falling again at the very end of its range (Fig. 1). Therefore, the cells traversed by the alpha particle are irradiated with a range of energies and LETs. The resulting human exposures are normally at very low dose rates to these very short densely ionizing tracks, with an average cell nucleus in the bronchial epithelium typically receiving around 0.002–0.009 alpha-particle traversals per year (*2*). However, while many cells are not traversed, those cells that are traversed receive a substantial local dose of up to ~0.5 Gy. Therefore, the

Editor's note. The online version of this article (DOI: 10.1667/RR13835.1) contains supplementary information that is available to all authorized users.

[1] Address for correspondence: CRUK/MRC Oxford Institute for Radiation Oncology, Gray Laboratories, University of Oxford, ORCRB, Roosevelt Drive, Oxford OX3 7DQ, UK; e-mail: mark.hill@oncology.ox.ac.uk.

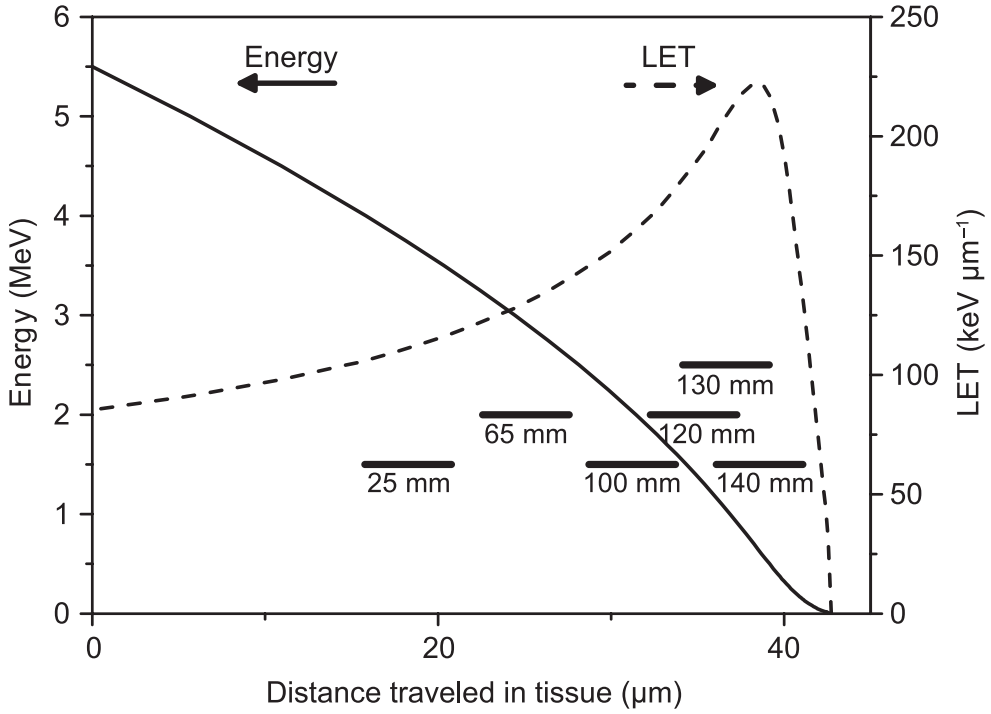

FIG. 1. Variation in energy and associated LET with distance traversed in tissue (assumed to be water) by a 5.5 MeV alpha particle (corresponding to energy of alpha particle emitted from a ^{222}Rn decay). Also shown is the approximate variation in energy and LET through a 5 μm thick cell (represented by bars) for the various experimental conditions described in this article, defined by the thickness of helium traversed in the irradiator used.

biological effectiveness of a single α-particle traversal is important.

With respect to medical exposures, there has been an increased interest in exploring the potential use of α-particle-emitting radionuclides in radiotherapy. In particular, there is current interest in the use of targeted alpha-particle therapy (TAT) for the treatment of micrometastases, which is achieved by targeting the α-particle-emitting radionuclide to cancer cells by attaching monoclonal antibodies (or other targeting molecules). This technique takes advantage of the short high-LET tracks produced, typically resulting in a high efficiency of cell inactivation and limiting damage to a small number of cells close to the point of decay, thereby minimizing damage to surrounding healthy tissue. As discussed in a recent review by Elgqvist *et al.* (*3*), a number of clinical trials have been reported for a variety of cancer types using a range of α-emitting radionuclides (including ^{213}Bi, ^{211}At, ^{225}Ac, ^{212}Pb/^{212}Bi and ^{223}Ra), which emit either single or multiple α particles depending on the decay chain, with energies ranging from 5.7 MeV up to 8.8 MeV. Again, irradiated cells are traversed by a range of energies and LETs as each α particle slows down, resulting in a variation in efficiency of cell inactivation.

The biological effectiveness of high-LET charged particles as a function of energy is also an important factor with respect to the increasing use of accelerated charged particle for therapy. This is particularly true for carbon ion therapy, for which there is a significant variation in relative biological effectiveness (RBE) with depth of the treatment beam as carbon ions lose energy and with the increasing contribution due to secondary ions resulting from fragmentation processes. A range of radiobiological models have been developed for use in conjunction with treatment planning software to take this variation into account and enable the optimization of the beam with respect to biological effect rather than absorbed dose. For proton therapy, the RBE is routinely assumed to be 1.1, however, experiments have shown that the RBE does vary with energy and significantly increases towards the very end of particle range (*4*). To develop and test these radiobiological models [e.g., LEM IV (*5*), RCR (*6*) and MCDS (*7*) models] it is important that experimental data are available for a range of energies (ideally including monoenergetic energies), particles and cell types. Although clinical treatments are currently restricted to protons and carbon ions, the potential of a range of different ions is also being explored (*6*).

The conventional picture of RBE variation with LET for a range of biological end points (*8*), including cell inactivation (*9, 10*), mutation (*11, 12*) and transformation (*13*), shows a sharp rise in RBEs from low-LET radiation (~several keV μm^{-1}) up to a peak at about 100–200 keV μm^{-1} and then decreasing at higher LET values. For a number of studies the experimental data are obtained using a range of particles to cover the required range in LET.

However, it is known that the different particles of the same LET will have different RBE values as a result of changes in the local ionization density due to differences in the energy spectra and range of δ-ray electrons produced along the track (*14*). Therefore, it is important whenever possible to use only the particle of interest, although this can be problematic in some cases due to the limited particle range. A limited number of studies have investigated the variation of RBE as a function of energy/LET of α particles. However, the determination of RBEs in these types of experiments depends very critically on estimating the ''true'' absorbed dose to the cell and to sensitive structures within the cell. This is not a trivial problem, since the α-particle energy and LET may change rapidly over the dimensions of the cell, especially as the α particle approaches the Bragg peak. The dimensions of the cell and its nucleus must be accurately known. The energy and angular distributions of the incident α particles must be well characterized, and their subsequent behavior must be understood as they continue to traverse the cell.

The Medical Research Council (MRC) plutonium-238 irradiator (now located at the Oxford Institute for Radiation Oncology, Oxford) is particularly well suited for the study of the variation in biological effectiveness with α-particle energy (*15*). It allows the irradiation of a cell layer with an essentially parallel beam of nearly monoenergetic α particles, with energies varying from 4.2 MeV down to 1 MeV and below, with corresponding LETs rising from 103 keV μm^{-1} up to the maximum of 237 keV μm^{-1} within the irradiated cell. In this study, the facility was characterized for six different irradiation conditions enabling incident energies from 4.0 MeV down to 1.1 MeV, with the incident dose determined by fluence measurements for each energy and cell morphology measurements determined to calculate the average absorbed dose to the cells. The variation in clonogenic survival of V79-4 cells was determined as a function of incident energy along with the relative variation in the initial yields of DNA double-strand break (DSB) induction measured using the fraction of activity released (FAR) assay. The results will expand on the previous data obtained at Harwell for the same V79-4 cells and culture techniques using helium ions with energies ranging from 5.85 MeV up to 34.9 MeV. In addition to the variation in RBEs for cell inactivation as a function of α-particle (helium ion) energy, the variation in the probability of surviving a single α-particle traversal is explored.

MATERIALS AND METHODS

Tissue Culture and Cell Survival

For each irradiation experiment, an ampoule of V79-4 Chinese hamster cells was recovered from the MRC stock in liquid N_2 storage, thawed and grown in T75 Eagle's minimum essential media (Gibco®; Life Technologies, Grand Island, NY) with 10% fetal calf serum (Sigma-Aldrich Company Ltd., Dorset, UK), 1 m*M* L-glutamine (Sigma-Aldrich) and penicillin/streptomycin (Sigma-Aldrich). Exponential growth was maintained for 3 days at 37°C in 5% CO_2/95% air. Cells were harvested with trypsin/EDTA (Becton Dickinson, Franklin Lakes, NJ), centrifuged, resuspended in growth media and counted before dilution to the required density. Approximately 2×10^5 cells in 2 ml were seeded into each irradiation dish. The dishes consisted of Pyrex® glass cylinders (25 mm deep, 30 mm internal diameter) with a thin Hostaphan® base (0.35 mg cm^{-2} polyethylene terephthalate; Hoechst, Franford, Germany) to allow passage of the α particles. Dishes were incubated for approximately 40 h prior to irradiation as a subconfluent, exponentially growing cell monolayer, with two dishes irradiated per dose point and cells pooled. Immediately after irradiation a 26 mm diameter disc was cut out from the base of each dish using a custom-made tool (*16*) and placed in trypsin/EDTA to remove cells. The cells were centrifuged, resuspended in growth media, counted and respread into 9 cm diameter petri dishes at densities expected to yield about 200 colonies per dish. After 8 days of growth, the colonies were fixed, stained with methyl blue and surviving colonies (>50 cells) counted. The fraction of surviving cells was calculated with respect to the cloning efficiency of the sham-irradiated cells. The resulting curve was fitted to the equation,

$$S/S_0 = \exp(-\alpha D) \tag{1}$$

where S/S_0 is the surviving fraction and D is the mean dose to an average cell.

DSB Induction

To determine the variation in initial yield of DSB as a function of α-particle energy, cells were prepared in irradiation dishes in an identical manner to the survival experiments and the assay performed is similar to that previously described (*17*). Approximately 24 h prior to irradiation, cells were labeled with tritiated thymidine (3 μl of stock solution consisting of 0.1 ml [^{3}H]thymidine) (Amersham International, Little Chalfont, UK) in 50 μl of free thymidine (1 mg ml^{-1} in water; Sigma-Aldrich) and 1.85 ml of phosphate buffered saline (PBS; Sigma-Aldrich). At least 1 h prior to irradiation the active media was replaced with fresh media and tritium free thymidine. Dishes were irradiated (mean doses ranging from 0 to ~20 Gy) at ~5°C and placed on ice immediately afterwards. Cells were harvested on ice and resuspended in 0.8% low-melting-point agarose in PBS and immediately pipetted into chilled plug molds and stored at 4°C, with 2 plugs per dose point. The plugs were subsequently removed from the molds and the cells lysed with ice-cold solution of proteinase K (0.05%), *N*-lauryl sulphate (2%) and 0.5 *M* dm^{-3} EDTA (Sigma-Aldrich) at pH 7.5 for 1 h at 4°C and then 24 h at 37°C. DSB induction was determined using the fraction of activity released (FAR) assay using pulsed-field gel electrophoresis (PFGE) (model no. CHEF DR11, Bio-Rad Laboratories Ltd, Hemel Hempstead, UK). The electrophoresis grade agarose gel (UltraPure™; Gibco) was prepared at 0.8% in TBE buffer (Sigma-Aldrich) and run for 96 h at 45 V with a 60 min switching time at 16°C. The gel was subsequently stained with 0.0 μg ml^{-1} ethidium bromide (Sigma-Aldrich) then washed with water. With the aid of an ultraviolet transluminator, the well and lanes for each plug were separated with the lane cut into five pieces. These were transferred into glass scintillation vials containing 0.5 ml of 1 *M* dm^{-3} HCl (Sigma-Aldrich) and heated to melt the gel. Once cool, ~7 ml of liquid scintillant (OptiPhase HiSafe 3; PerkinElmer® Inc., Woodbridge, Canada) was added and mixed by vortexing. The activity in each vial was determined using a Beckman LS6500 scintillation counter [Beckman Coulter Ltd., High Wycombe, UK]. The relative yield of DSB was determined by the amount of DNA extracted from the cell given by the fraction extracted:

$$FE = \frac{C_{lane}}{C_{lane} + C_{well}} \tag{2}$$

where C_{lane} and C_{well} represent the total counts per min in the lane and well, respectively.

TABLE 1
Beam Characteristic as a Function of Helium Distance Traversed by the α Particles

Helium depth (mm)	Mean energy at cell entrance ± HWHM (MeV)	Residual range (μm)	Mean α-particle fluence (cm^{-2} rev^{-1})	Entrance ''dose rate'' (Gy rev^{-1})	Mean ''dose rate'' to cell (Gy rev^{-1})	Average LET across cell (keV μm^{-1})	Range of LET across cell (keV μm^{-1})	Range of LET across nucleus (keV μm^{-1})
25	4.0 ± 0.2	26	8.488×10^5	0.145	0.151	112	106–117	107–116
65	3.2 ± 0.2	19	2.490×10^6	0.488	0.522	131	123–141	124–138
100	2.4 ± 0.3	13	1.085×10^6	0.254	0.280	161	146–180	149–175
120	1.8 ± 0.3	9.8	7.610×10^5	0.205	0.231	190	168–210	172–207
130	1.5 ± 0.4	7.9	6.510×10^5	0.193	0.210	201	185–191[a]	190–203[a]
140	1.1 ± 0.4	6.0	5.630×10^5	0.180	0.163	181	200–116[a]	202–143[a]

Notes. Including mean energy of alpha particles incident on the cell monolayer along with half-width at half-maximum (HWHM); residual range; mean fluence averaged over cell monolayer; incident dose per wheel revolution; mean dose per wheel revolution for a 5 μm thick cell; average LET across the cell; average LET entering and exiting the cell; and average LET entering and exiting the nucleus.

[a] Reaching a maximum value for LET part way through the nucleus.

Cell Characteristics

Accurate knowledge of cell dimensions is needed for dosimetric purposes. Therefore, cell morphology measurements were performed on live cells in spare irradiation dishes at the time of irradiation using a confocal laser-scanning microscope [Bio-Rad Lasersharp MRC-600 on a Nikon® Diaphot inverted microscope (Nikon Instruments Inc., Melville, NY) with an ion argon laser operating at 488 nm]. Cell thickness measurements were performed by adding FITC-dextran (Sigma-Aldrich) to the dish as previously described (*18, 19*). Confocal microscopy measurements were also used to measure nuclear areas of live cells using $DIOC_6$ (3,3′-dihwxyloxacarbocyanine iodide; Sigma-Aldrich) vital mitochondrial stain, as previously described by Townsend and Marsden (*20*). Most mitochondria are found close to the nucleus, so allowing the perimeter of each nucleus to be identified and drawn around manually enabled the confocal analysis software to calculate the nuclear area through the middle of a cell. To assess cell cycle status at the time of irradiation, cellular RNA was measured with Becton-Dickinson FACSort™ in a procedure more fully described by Hill *et al*. (*21*).

Alpha Irradiations

Alpha-particle irradiations were performed using the MRC ^{238}Pu α-particle source, previously described in detail by Goodhead *et al*. (*15*). The 5.5 MeV α particles are emitted from a thin (0.67 mg cm^{-2}) uniform 20 mm diameter layer of ^{238}Pu plated on a platinum disc. The α particles pass through a helium-filled chamber maintained at atmospheric pressure, before exiting through a 0.35 mg cm^{-2} Hostaphan window, traverse a 3.0 mm air gap and enter the irradiation dish through its Hostaphan base. Up to 10 irradiation dishes were placed on a rotating wheel, which rotated at 3.00 rev/min^{-1} until the required dose was delivered. The dishes pass over a selectable sector plate, which defines the edges of the exit beam and ensures that all positions on an irradiation dish are exposed for the identical length of time. The dose delivered is determined by the number of revolutions of the wheel, the angle subtended by the sector plate and the size of the aperture situated just above the source. For these experiments all irradiations were performed with a sector plate that subtended 24° at the wheel center and with the largest aperture of 25 mm diameter (so the source was fully uncovered), apart from when the helium distance was 25 mm when a 4.5 mm diameter aperture was used. The use of helium in the chamber allows a greater source to target distance than what could be achieved in air (helium is about 7 times less dense than air). The result is that all α particles enter the cell layer at approximately normal incidence and with approximately the same energy. Additionally, by adjusting the source position, the distance traversed through the helium gas can be varied from 10–160 mm, giving α-particle energies at the cell layer from about 4.2 MeV down to zero. In this experiment, distances in helium of 25, 65, 100, 120, 130 and 140 mm were used to produce six bands of alpha energies and LETs, covering almost all of the α particle stopping power curve. The energy distributions at the entrance to the cell layer were measured with a silicon surface barrier detector (UK Atomic Energy Authority Research Establishment, Abingdon, UK) coupled to an ADC and pulse height analyzer system (AccuSpec; Canberra Industries Inc., Meriden, CT).

The fluences at the various source positions were measured by irradiating discs of CR39 plastic (same diameter as the dishes) in the identical geometry to the cell irradiations. The exposed CR39 discs were etched with 60% KOH solution at 60°C for about 90 min to develop clearly visible tracks that could be counted under a microscope. The variation in track density as a function of distance from the center of the dish (along a line which would intercept the axis of rotation of the wheel) was determined for each of the helium distances used. The resulting distribution was then used to calculate the average fluence per revolution across a 26 mm diameter area central to the dish.

For each source position, two dishes were irradiated per dose group. Every attempt was made to treat the control cells identically to the irradiated cells. This included a sham irradiation of the control cells, achieved by placing them on the irradiation wheel and blocking the α particles with brass plates.

Dose Determinations

Due to loss of energy of the α particles as they traverse the cell, and corresponding increase in LET, the mean dose to the cell is different to the dose on the incident surface of the cell. The dose at a given depth within the cell is given by:

$$D = \Phi L/\rho \tag{3}$$

where ρ is the density, Φ is the particle fluence and L is the LET [this corresponds to D (Gy) = 0.16 * Φ (particles μm^{-2}) * L (keV μm^{-1}) assuming a cell density of 1 g cm^{-3}].

The average dose within the cell nucleus was calculated as follows. Each energy distribution for a given helium distance (see below) was multiplied by the appropriate fluence (Table 1) for that energy distribution. In this way each channel of the energy spectrum gave the number of alpha particles entering the cell layer within a certain energy interval. For a given energy interval, alpha particles were followed through the cell layer calculating the energy loss at successive 0.1 μm intervals using the SRIM stopping power data for helium ions in water (*22, 23*) and so giving the variation in LET and absorbed dose as functions of depth in the cell layer. The resulting doses were summed over the entire energy spectrum and averaged throughout the depth of the cell nucleus:

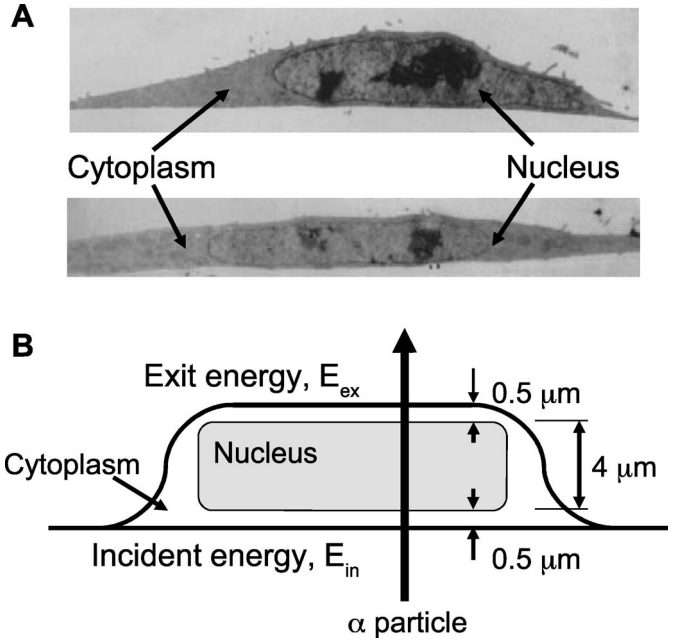

FIG. 2. Panel A: Examples of typical electron micrograph sections of attached V79-4 cells. Panel B: Schematic of cell geometry assumed for calculations.

$$\overline{D} = \frac{\sum_i \sum_j \Phi(E_i) L_{ij}}{\rho \sum_j 1} \tag{4}$$

where $\Phi(E_i)$ is the fluence of particles in the energy interval E_i to E_{i+1} entering the cell layer covering the whole energy spectrum and L_{ij} is the LET for the depth interval j to $j + 1$ in the cell layer for incident energy E_i, which is summed from the incident surface to a distance corresponding to the average height of a cell.

RESULTS

Cell Characteristics

The electron micrograph in Fig. 2A shows the attached V79 cells to have a flat, pancake shape with the nucleus approximately elliptic cylindrical in shape. From analysis of these micrographs the average ratio of nuclear to cell thickness was estimated to be 0.8. Electron micrographs by themselves cannot be relied upon to give accurate values of cell thickness because of shrinkage during preparation (*18, 19*). From the confocal laser-scanning microscope measurements on live cells, a mean cell thickness of 5.0 μm (standard deviation = 1.2 μm) was obtained from 111 cells analyzed, with the distribution in cell heights shown in Fig. 3A. Therefore, for the dose calculations detailed below an average cell thickness of 5.0 μm was assumed. A nuclear height of 4.0 μm, with 0.5 μm of cytoplasm above and below the nucleus was also assumed (Fig. 2B). A mean nuclear area of 113 μm² (standard deviation of 34 μm²) was obtained from the analysis of 469 cells, with Fig. 3B showing the wide distribution in the measured areas. Cell cycle analysis performed on cells grown in Hostaphan-based irradiation dishes at the time of irradiation showed that on average 55–60% of the cells were in G_0/G_1 phase, 10–12% were in G_2 phase and 28–35% were in the S phase.

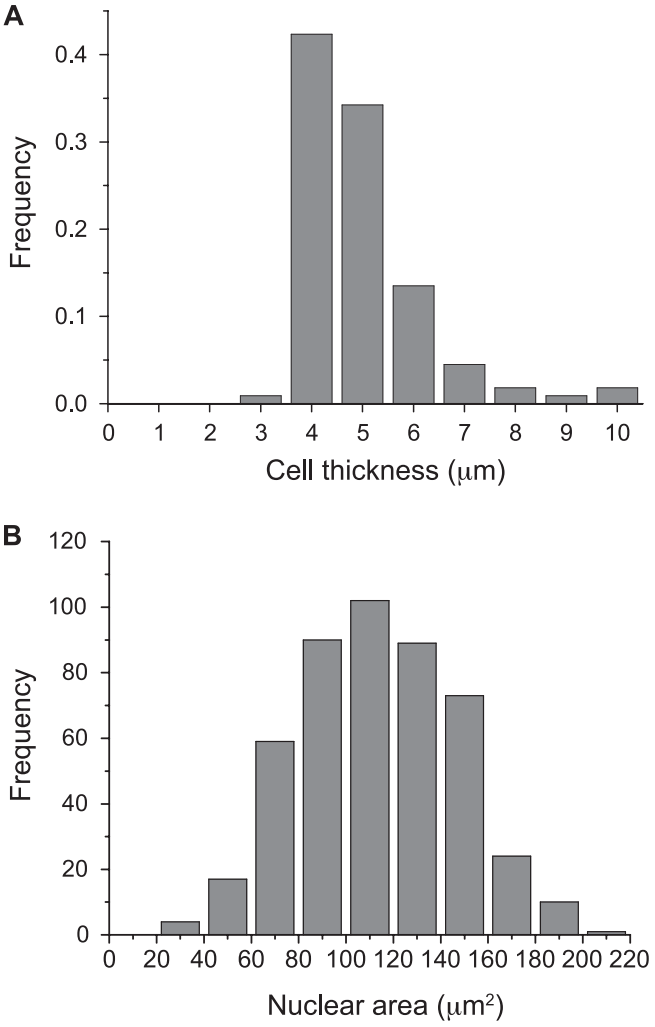

FIG. 3. V79-4 morphological measurements. Panel A: Cell height distribution from 111 cells, giving a mean height of 5.0 μm (SD = 1.2 μm). Panel B: Nuclear area distribution, giving a mean nuclear area of 113 μm² from 469 cells (SD = 34 μm²).

Beam Characteristics and Dose Determination

Figure 4 shows the spectra of α-particle energy as a function of helium traversed, with the calculated mean incident energies shown in Table 1. From the CR39 measurements, the calculated mean fluence of α particles across the central 26 mm of the irradiation dish per revolution of the wheel holding the dishes is shown in Table 1 for each of the helium depths used, along with the incident dose rate on the surface of the cells. For helium distances of 65 mm and above, the CR39 measurements showed minimal variation across the central 26 mm of the dish,

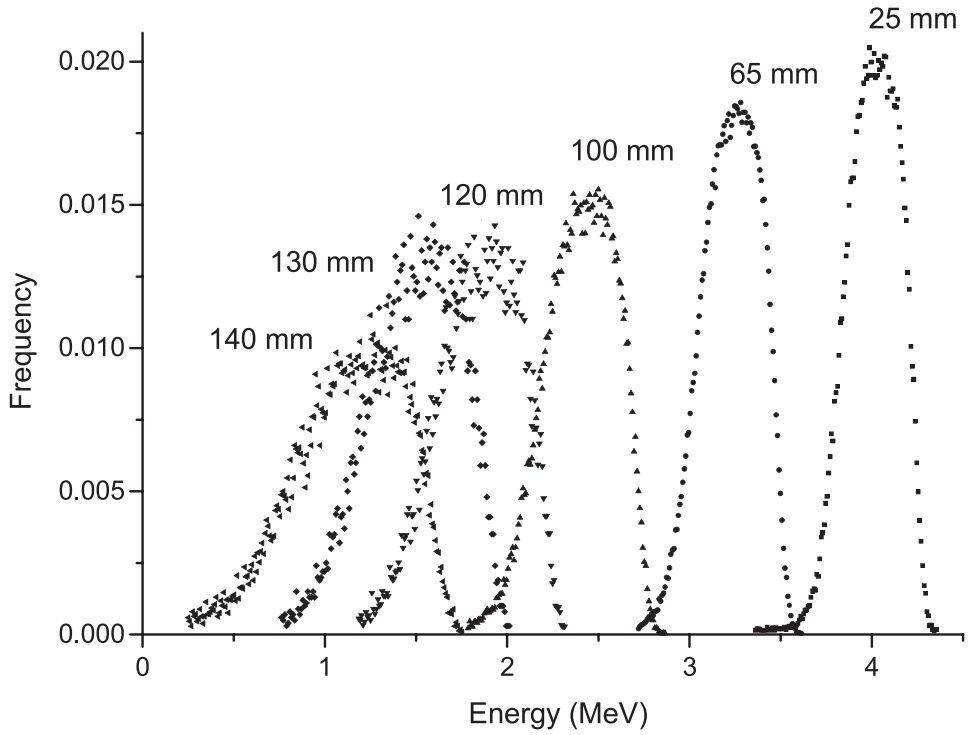

FIG. 4. Spectra of alpha-particle energies incident on the cell monolayer for the specified distances of helium traversed (25–140 mm). The associated mean energy and half-width at half-maximum values are shown in Table 1.

while for 25 mm of helium a correction factor of 0.927 was used to account for the observed variation (see Supplementary Fig. S1; http://dx.doi.org/10.1667/RR13835.1.S1). Assuming a mean cell height of 5 μm (Fig. 3A) and the incident α-particle spectra shown in Fig. 4, the calculated mean dose rate to the cell and average LET are tabulated in Table 1 along with the range of LET values experienced by the cell as the α particle traversed the cell or nucleus.

Clonogenic Survival

Figure 5 shows the V79-4 clonogenic survival curves as a function of α-particle energy, determined by the source position. Table 2 shows the corresponding fitting parameters. The results for the 3.2 MeV (helium depth of 65 mm) showed good agreement with experimental data previously published by Hill *et al.* (*24*) when plotted using mean dose to a 5 μm thick cell; the data were combined for subsequent analysis. While the survival curve for the two highest energies used (4.0 MeV and 3.2 MeV) resulted in similar survival curves (with 3.2 MeV slightly more effective), further decreasing the energy of the α particles (with associated increase in LET) resulted in an increase in survival for a given dose. The RBE was calculated by comparing to the previously published ^{60}Co γ-ray data obtained using the same V79-4 cells (*25*) and described by the equation:

$$S_\gamma/S_{\gamma 0} = \exp[-(0.143 \pm 0.015)D - (0.0259 \pm 0.0019)D^2] \quad (5)$$

Table 2 shows the resulting RBE values obtained for the 10% survival, as well as the maximum low-dose RBE (RBE_M) determined as the ratio of the initial slopes of the dose-effect curves for the current radiation study to that of the γ-ray reference radiation. The RBEs increase with increasing level of survival due to the curvature of the γ-ray survival curve. Also included in Table 2 are the experimental data obtained for the same V79-4 cells (*11, 25*) performed using the Variable Energy Cyclotron or the Tandem Van de Graaff accelerator, which were formerly operated by the UK Atomic Energy Authority at the Harwell Research Establishment (*26*). The RBE values presented are also calculated with respect to the same ^{60}Co γ-ray data (*25*) used for the current data. The variation in RBE as a function of incident α-particle energy and LET for the combined data set are shown graphically in Fig. 6. The data shows a peak in the RBE value for incident energies of around 3.2 MeV and corresponding average LET of 131 keV μm^{-1}.

For a random (Poisson) distribution of numbers of tracks per cell the average number of tracks, N, traversing a mean nuclear area A (in μm^2) for a given dose D (in Gy) is given by

$$N = \frac{AD}{0.16L} \quad (6)$$

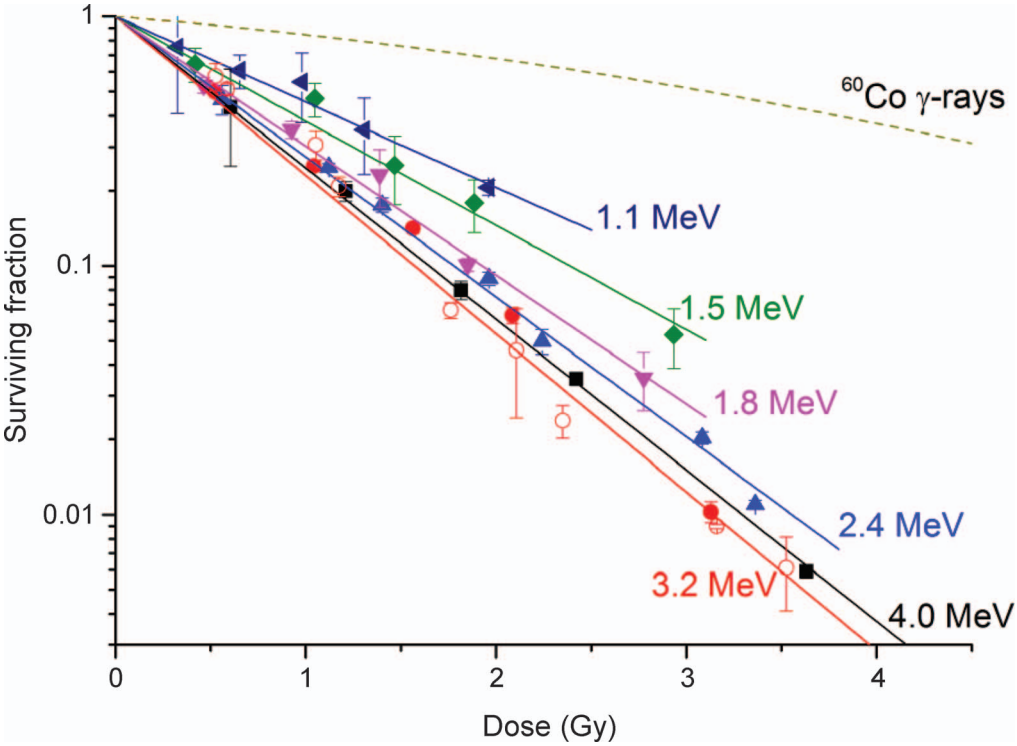

FIG. 5. Survival of V79-4 cells as a function of alpha-particle energy: (■) = 4.0 MeV (25 mm of He); (●) = 3.2 MeV (65 mm of He); (○) = 3.2 MeV [65 mm of He, previously published data (*24*)]; (▲) = 2.4 MeV (100 mm of He); (▼) = 1.8 MeV (120 mm of He); (◆) = 1.7 MeV (130 mm of He); (◀) = 1.1 MeV (140 mm of He). The previously published ^{60}Co γ-ray survival data for V79-4 cells is also shown (*25*). Errors bars represent standard error of the mean.

where L is the LET in keV μm^{-1} and assuming unit density. The mean probability, S_1, of survival after a single α-particle traversal through the cell nucleus can be estimated (*27, 28*) with the mean nuclear area and the mean lethal dose D_0, using the equation,

$$S_1 = 1 - \left(\frac{0.16L}{AD_0}\right) \tag{7}$$

TABLE 2
Variation in the RBE for 10% Survival ($RBE_{10\%}$), Maximum Low-Dose RBE (RBE_M) and Associated Parameters as a Function of Alpha-Particle (Helium Ion) Incident Energy and Average LET to the Cell

Data set	Incident energy (MeV)	Average LET (keV μm^{-1})	Fitted α-coefficient (Gy^{-1})	RBE_M[a]	$RBE_{10\%}$[a]	N/D (Gy^{-1})	S_1	l_1	l_D
Original Harwell	34.9	20.85[b]	0.491[c]	3.4[d]	1.7[d]	33.9	0.99	0.015	0.49
data (*11, 25, 26*)	24.3	28.2[b]	0.549[c]	3.8[d]	2.1[d]	25.0	0.98	0.022	0.56
	11.7	51.5[b]	0.933[c]	6.5[d]	3.0[d]	13.7	0.93	0.070	0.97
	7.6	72[b]	0.961[c]	6.7[d]	3.6[d]	9.8	0.90	0.103	1.01
	5.85	87.7[b]	1.29[c]	9.0[d]	4.3[d]	8.1	0.84	0.175	1.41
Current data	4.0	112	1.398 ± 0.023	9.8 ± 0.2	4.29 ± 0.07	6.3	0.78	0.251	1.58
	3.2	131	1.463 ± 0.023	10.2 ± 0.2	4.49 ± 0.07	5.4	0.73	0.317	1.71
	2.4	161	1.295 ± 0.018	9.1 ± 0.1	3.97 ± 0.06	4.4	0.70	0.350	1.54
	1.8	190	1.195 ± 0.032	8.4 ± 0.2	3.67 ± 0.10	3.7	0.68	0.388	1.44
	1.5	201	0.965 ± 0.036	6.7 ± 0.3	2.96 ± 0.11	3.5	0.73	0.321	1.13
	1.1	181	0.789 ± 0.065	5.5 ± 0.5	2.42 ± 0.20	3.9	0.80	0.226	0.88

Notes. The current data are fitted to $S/S_0 = \exp(-\alpha D)$, while the original Harwell data were fitted to $S/S_0 = \exp(-\alpha D - \beta D^2)$ and only the alpha-coefficient corresponding to the initial slope is shown. Also tabulated are the average number of nuclear traversals per Gy, N/D, the mean probability of surviving a single alpha-particle traversal, S_1, the average number of lethal lesions per track, l_1, and corresponding lethal lesions per unit dose, l_D.

[a] RBE calculated with respect to ^{60}Co γ-ray data fitted to $S/S_0 = \exp(-\alpha D - \beta D^2)$, where $\alpha = 0.143$ Gy^{-1}, $\beta = 0.0259$ Gy^{-2} and dose for 10% survival, $D_{10\%}$ of 7.06 Gy (*25*). Uncertainties shown reflect only the uncertainties in the α-particle data and not the γ-ray data.

[b] Average across a 7 μm cell.

[c] The original Harwell survival data were fitted to a linear-quadratic equation $S/S_0 = \exp(\alpha D - \beta D^2)$.

[d] RBEs for Harwell were calculated using absorbed dose to entrance surface of cell.

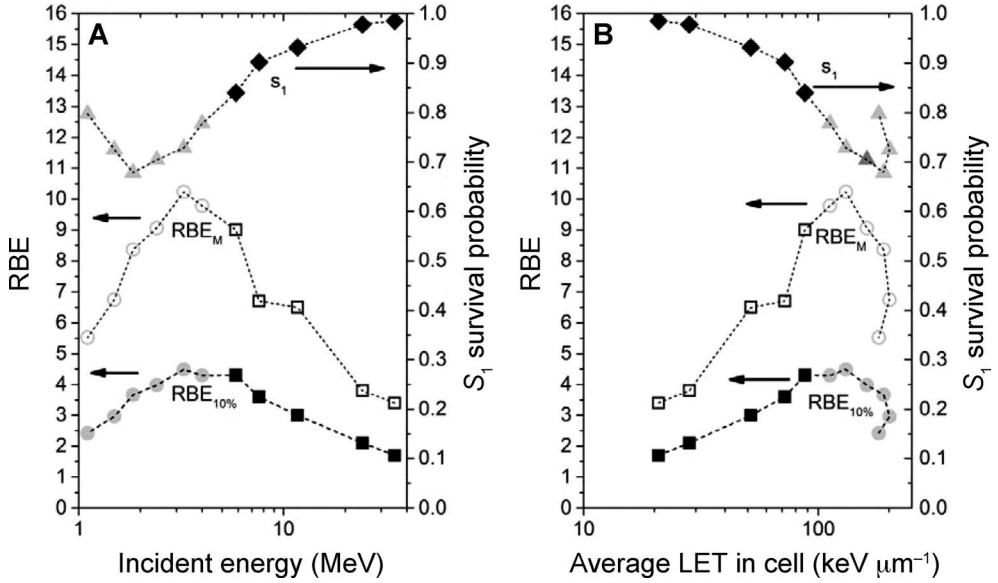

FIG. 6. Variation in RBE for 10% survival ($RBE_{10\%}$), maximum low-dose RBE (RBE_M) and the calculated probability, S_1, of surviving a nuclear traversal by a single alpha-particle track as a function of incident energy (panel A) and average LET (panel B) in the cell. Circles and triangles represent current data, while squares and diamonds represent original Harwell data.

As described by Goodhead *et al.* (*28*) the exponential survival curve $S/S_0 = \exp(-\alpha D)$ can be represented by

$$S/S_0 = \exp\{-N[1 - \exp(-l_1)]\}, \tag{8}$$

where l_1 is the average number of lethal lesions randomly distributed along a track through a cell nucleus. Therefore, the average number of lethal lesions per track is given by

$$l_1 = -\ln\left(1 - \frac{0.16L\alpha}{A}\right) \tag{9}$$

and the number of lethal lesions per unit absorbed dose as

$$l_D = \frac{N}{D} l_1 = \frac{A}{0.16L} l_1 \tag{10}$$

It is worth noting that the quantities l_1 and l_D provide estimates of an ''intrinsic radiosensitivity'' to the α-particle-induced damage taking into account the effects of potential multiple lethal lesions along individual tracks. Based on an average nuclear area of 113 μm^2, the calculated number of nuclear traversals per Gy, the mean probability of surviving a single α-particle traversal, S_1, the average number of lethal lesions per track, l_1, and corresponding lethal lesions per unit dose, l_D, are tabulated for both the present data and the previous Harwell data in Table 2. The variation in S_1 as a function of energy and LET is shown graphically in Fig. 6. These data show that α particles with incident energy of around 1.8 MeV (average LET of 190 keV μm^{-1}) are the most lethal with respect to single α-particle traversals with the corresponding highest number of lethal lesions per track, l_1.

The variation in the relative yield of initial DSB measured using the FAR assay is shown in Fig. 7, normalized to the 3.2 MeV data (where the relative yield is defined as 1) for comparison with previous data from MRC Harwell obtained showing an RBE for DSB induction in V79-4 cells of between 0.85 using sucrose sedimentation (*29*) and 1.0 using PFGE (*30*) for α particles of similar energy. The data is plotted as both the relative number of DSB per Gy and the relative number of DSB per track. As the energy of incident α particles decreases, this data suggests that although there appears to be slight decrease in the measured yield of DSB per Gy, the yield of DSB per nuclear traversal increases.

DISCUSSION

A number of experimental studies have been performed over the years examining the variation in biological effectiveness of charged particles at inducing cell inactivation as a function of particle energy (LET) for a range of different particles and cell types. Much of this work has now been compiled in the Particle Irradiation Data Ensemble (PIBE) database, which contains information on over 800 cell experiments from laboratories around the world (*31*). The RBE is not a single value for a given LET, but is also dependent on the level of biological effect at which the comparison is made, the cell type, growth conditions and environment, reference radiation and the particle type (*8*). The variation in biological effectiveness for different particles with the same LET is due to differences in the track structure and variation in local dose along the track because of different ranges of the δ electrons.

As shown in Fig. 8, the variation in RBE for 10% survival with LET for the α-particle V79-4 survival data presented in this article [which includes the data previously obtained with the same cells for helium ions at Harwell (*11, 25*)]

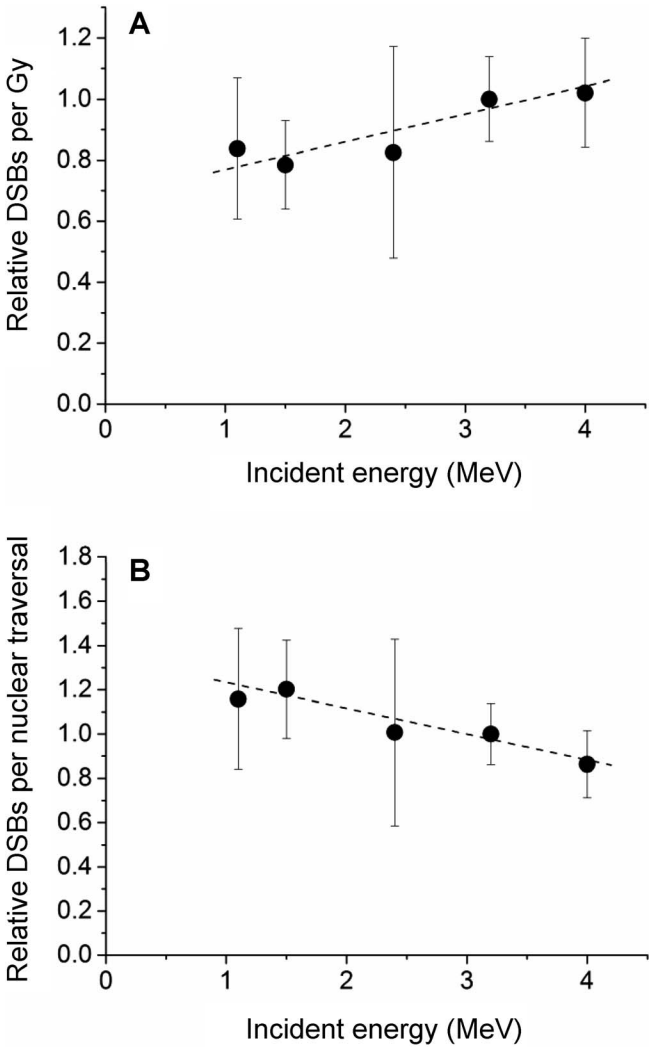

FIG. 7. Variation in the relative yields of initial DSB as a function of incident energy of the alpha particles (helium ions) per unit dose (panel A) and per nuclear traversal (panel B). The values have been normalized to 3.2 MeV.

compares well with other published V79 survival data for helium ions (closed symbols joined by lines). The data presented for Folkard *et al*. (*4*) and Furusawa *et al*. (*32*) was produced using ^{3}He ions rather than ^{4}He ions. Folkard *et al*. irradiated cells as an unattached monolayer with minimal media and the cells were assumed to be partially flattened spheres approximately 10 μm thick. Although V79 cells are not of human origin, this and previous data (*24*) showed that these cells represent a sensitive and reproducible assay useful for mechanistic studies.

In addition, Fig. 8 shows good agreement with the variation in RBE for survival after helium ion irradiation for a range of other cell lines (open symbols). The data for primary human fibroblast HF19 cells (*12, 25*) were also obtained at Harwell. Interestingly, for these cells the corresponding 250 kVp X-ray survival curve was also observed to fit to the equation $S/S_0 = \exp(-\alpha D)$ and therefore the RBE is independent of survival level used for the comparison (dose). Figure 8 also includes data on human kidney T-1 cells (*9, 33*) (cells assumed to be 4 μm thick), C3H 10T1/2 cells (*13*) and human salivary gland (HSG) tumor cells (*32*). The data for the 75 keV μm^{-1} point for the C3H 10T1/2 cells and all the points for HSG cells were also obtained using ^{3}He ions. Where values or fits were not readily available from the original data the survival curve fit coefficients in the PIDE database were used to calculate the RBE. For low-incident energy particles (high LET) towards the end of their range, the cell morphology can be a major factor in not only the biological response but also the calculated LET and associated calculation of dose due to the large variation in LET through the cell (see Fig. 1).

The data presented in this article for the variation of RBE as a function of LET shows the curve ''curling back'' on itself, indicating that more than one value of RBE may be obtained by particles with the same LET but different energies. Although difference may be expected from the fact that the energy and associated range of δ rays produced by the lower energy alpha particles will be less than those produced by higher energy α particles of a similar LET, there are additional considerations that need to be taken into account when interpreting the 1.1 MeV data. The LET for these α particles varies significantly through the cell, with an incident LET of ~200 keV μm^{-1} rising to a maximum of ~237 keV μm^{-1} before falling to ~116 keV μm^{-1} on the exit surface of 5 μm thick cell (Table 1). In addition, because of the variability in the range of individual α particles together with the variation in thickness of individual cells (Fig. 3A), the exit LET will vary significantly and for a fraction of cells not all of the α particles will fully traverse the cell or nucleus.

As the energy of the α particle (helium ion) decreases, there is an increase in LET resulting in an increase in the average number of lethal lesions per track, l_1, and associated decrease in survival probability after a single particle traversal, S_1 (Fig. 6, Table 2). At low energies this increase is associated with an increase in the average absorbed dose per traversing track and increasing number of DSBs and associated complexity of the DSB [see Nikjoo *et al*. (*34*) and Fig. 7B]. As the α particle slows down to energies less than 0.65 MeV, the LET starts to fall with decreasing energy. This becomes important in this experiment when the incident energy is less than ~1.8 MeV when the peak of LET lies within the 5 μm thick cell (Fig. 1) leading to a reduction in l_1 values and associated increase in S_1 (Table 2). Although the effectiveness of individual tracks at inactivating the cell typically increases with decreasing incident energy, the number of traversals per unit absorbed dose decreases. The data show for the experimental set-up used, that the maximum number of lethal lesions per unit absorbed dose, l_D, is obtained for incident energies of 3.2 MeV, resulting in a peak in the RBE values.

Although the RBE-LET relationship for α particles is quite similar for the variety of cell lines shown in Fig. 8, it is

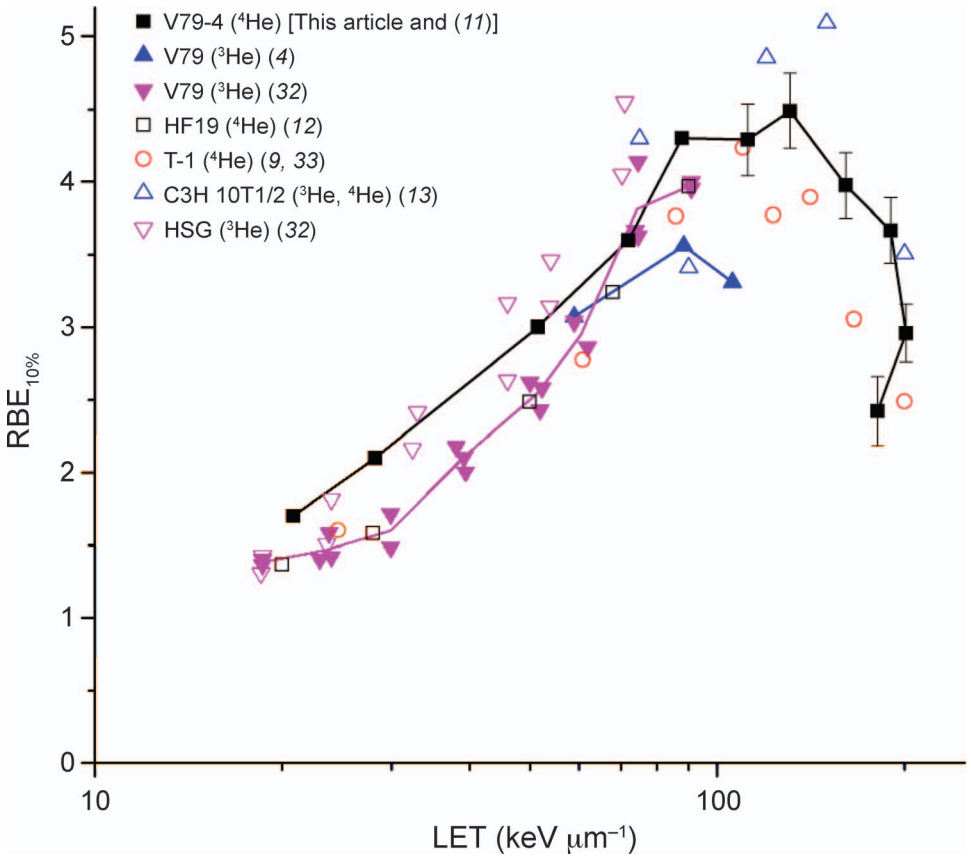

FIG. 8. Variation in RBE for 10% survival as a function of LET of helium ions (^{3}He and ^{4}He) for a range of experimental data on V79 cells (closed symbols) and other cell lines (open symbols).

likely to vary substantially for other cell types, particularly for those of greater intrinsic radiosensitivity and/or with compact nuclei (*24, 35, 36*). The variation will be reflected also in the single-track survival probabilities, S_1. For example, from previous experimental data with the same α-particle irradiator, it was estimated that, for α particles of LET 120 keV μm^{-1} the survival probability, S_1, varied from a value indistinguishable from zero for primary pre-B cells from Balb/c mice to about 0.8 for C3H 10T1/2 mouse fibroblasts (*37*). Evaluation of the effectiveness of the α-particle tracks for a given cell line in terms of number of lethal lesions per track, l_1, and hence effectiveness per unit track length, provides a means for estimating the sensitivity of the cells per unit dose if irradiated in other geometries, including along the long axis of flattened cells.

Ionizing radiation deposits its energy along highly structured tracks of ionization and excitation events, with the pattern varying not only on the nanometer/DNA scale, but also on the scale of the cell and tissue, and differences across all of these three scales can have a significant impact on the ultimate biological response. As for DNA damage, the increasing LET of the α particle (helium ions) with decreasing energy not only increases the frequency of clustering damage to DNA, but also the degree of complexity of the damage at the site, and it has been proposed that this is the main factor driving the differences in biological effectiveness between different radiation qualities for a range of biological end points (*38, 39*) including cell survival. For low-LET radiation, such as X rays or γ rays, the majority of DSBs produced are simple. Monte Carlo calculations estimate that the percentage of DSBs that are complex by virtue of an additional strand break within 10 bp (defined as DSB_C) was ~20%, rising to ~50% (*40, 41*) if the possibility of a base damage within 10 bp is also included in the definition of complexity (defined as DSB_{CB}). Similar calculations performed on helium ions (*34*) show that as the energy decreases from 10 MeV down to 2 MeV there is an increase in the local clustering of damage with the percentage of DSBs classified as complex (DSB_C) increasing from 45–73% (corresponding values for DSB_{CB} increase from 84–96%). This difference in the complexity of DSBs produced by α particles compared to gamma rays is reflected in the significant reduction in the extent of DSB rejoining. Previous experiments with V79-4 cells showed that ~90% of the DSB were rejoined 3 h after gamma-ray exposure, while only 30% were rejoined 3 h after exposure to 3.3 MeV α particles for a dose giving the same number of initial DSB (*42*).

Due to the deposition of energy along narrow densely ionizing tracks, and the additional complexity of damage produced at a single site on DNA, α particles have the potential to produce correlated sites of damage across higher

orders of DNA packing. Such packing includes DNA wrapped around nucleosome (~10 nm diameter), packaging of these nucleosomes into chromatin fiber (~30 nm wide) and these fibers arranged in loops. Correlated DSBs can lead to the production of DNA fragments, the existence of which have been experimentally demonstrated (*43, 44*) and supported by theoretical calculations (*45*). Most DSB assays, including the FAR assay used in our study, are not able to resolve these correlated events, and thus have a tendency to underestimate the actual yield of DSB (*44–46*). To some extent this can be addressed using fragmentation analysis to separate out and quantify as many of the small fragments as possible, however, to obtain the required sensitivity a very high dose is needed, which complicates the analysis of the results because of the multitrack effects. Studies by Belli *et al*. (*47*) on V79 cells using helium ions (123 keV μm^{-1}) showed that while the conventional FAR assay gave an RBE for DSB induction between 0.8 and 1.0, analysis using fragmentation counting gave an RBE of 1.2. Similar studies by Newman *et al*. (*48*) again irradiating V79 cells with α particles (110 keV μm^{-1}), for conventional FAR analysis or applying random-breakage fits gave an RBE for DSB induction of 0.6–0.8, while summing the number of DNA fragments in the range of 10 kpb–5.7 MBp gave an RBE of 1.7. Therefore, although Fig. 7A suggests a slight increase in the yield of DSBs per nuclear traversal with decreasing energy, the DSB yield is expected to increase significantly.

It has also been shown that track structure is important on the scale of the cell. Within the interphase nucleus of a human cell, the DNA is in the form of 23 pairs of chromosomes and each of these has been shown to occupy discrete domains with limited overlap (*49*) and typically with a nonrandom relative distribution of these within the nucleus (*50, 51*). High-LET α particles deposit energy along discrete, narrow, densely ionizing tracks with 90% of the energy deposited within ~10 nm (*52*) of the particle path due to the short range of the δ electrons. This very heterogeneous pattern of energy deposition results in highly correlated damage sites, including DSBs along the path of the alpha particle within and between the traversed chromosome domains. The resulting radiation-induced chromosome aberrations are critically dependent on the spatial distribution of these DNA damage sites and therefore the track structure. The movement of DSB within the nucleus has been shown to be limited to less than ~1 μm (*53, 54*). Studies in human peripheral lymphocytes (PBLs) have shown that the passage of individual alpha particles is efficient at inducing complex chromosome rearrangements (involving 3 or more breaks in 2 or more chromosomes) in contrast to low-LET X rays, which produce mainly simple rearrangements (no more than 2 breaks in 2 chromosomes) at low doses (*55, 56*). The vast majority of the complex aberrations produced are nontransmissible and therefore are lethal to the cell. A similar response was observed in human $CD34^+$ hemopoietic cells irradiated with a mean of ~1 alpha-particle track per cell with incident energies of 3.8 MeV, 3.3 MeV and 2.2 MeV and corresponding mean LETs through the cell of 119, 135 and 182 keV μm^{-1}. It was observed that with increasing LET of the alpha particle, there was an increase in the ratio of complex to simple aberrations (*57*). This increase in the proportion of complex aberrations with LET per alpha-particle traversal is a result of the increasing number of DSBs per track (support by the data shown in Fig. 7, which will be an underestimate of the actual increase due to the production of DNA fragments) and corresponding decrease in the average separation distance between these breaks (*57*). In addition, this may be aided by an increase in the complexity of the damage at individual sites and also a potential increase in probability of production of short DNA fragments. At higher doses, where there are multiple nuclear traversals, there is an increasing probability of rearrangements between sites of DNA damage produced by independent tracks or two tracks traversing the same chromosome domain producing two independent exchanges but connected by the common chromosome (*58*). However, both PBL and $CD34^+$ cells have a spherical geometry and relatively small nuclear volumes. The yield and complexity of the resulting aberrations are dependent on nuclear geometry and the orientation of the traversing high-LET particle (*59, 60*). This results in a variation in the number of DSBs induced within the nucleus per track and the number of chromosome domains traversed.

SUMMARY

The MRC ^{238}Pu α-particle irradiator has been calibrated to enable studies investigating the variation in biological response with incident energies ranging from 4.0 MeV down to 1.1 MeV. This facility has initially been used to investigate the variation in effectiveness of alpha particles at inactivating V79-4 cells as a function of energy, extending the previously published data obtained at Harwell using the same cells irradiated with helium ions with energies ranging from 34.9 MeV to 5.85 MeV. These studies were performed in conjunction with cell morphology measurements on live cells, enabling precise determination of absorbed dose and calculation of the average LET. The increased biological effectiveness per absorbed dose above that of gamma rays for these alpha particles (helium ions) is a result of the increased ability of these densely ionizing particles to produce clustered damage to DNA and associated decrease in repairability of the damage. As the particle slows down and LET increases this can lead to an increase in the number of DSBs (after accounting for correlated breaks resulting in short DNA fragments) and in the complexity of the DSBs produced. In addition, correlation of damage, such as DSBs, along the path of the particle leads to an increased probability of producing complex chromosomal rearrangements that, more often than not, are nontransmissible at mitosis and lead to cell death. The results show an increase

in RBE for cell inactivation with decreasing helium ion energy (increasing LET), reaching a maximum for incident energies of ~3.2 MeV and corresponding average LET of 131 keV μm^{-1}, above which the RBE is observed to fall at lower energies (higher LETs). The variation in RBE with LET shows good agreement with the limited published data for helium ions for the range of energies/LETs studied. The effectiveness of single alpha-particle traversals (relevant to low-dose exposure) at inducing cell inactivation was observed to increase with decreasing energy to a peak of ~ 68% survival probability for incident energies of ~1.8 MeV (average LET of 190 keV μm^{-1}) producing ~0.39 lethal lesions per track through the cell nucleus. However, the efficiency of single traversals will also vary significantly with cell morphology and angle of incidence, as well as cell type.

SUPPLEMENTARY INFORMATION

Fig. S1. Variation in fluence with distance from the center of the dish for irradiations performed with a helium depth of 25 mm (panel A) perpendicular to the wheel motion and (panel B) tangential to the wheel motion.

ACKNOWLEDGMENTS

The authors wish to acknowledge the contribution of TJ Jenner and Sarah Livermore for their help performing the DNA DSB experiments and KMS Townsend in carrying out the confocal microscope measurements and cell cycle analysis. The work was partially supported by Medical Research Council Strategic Partnership Funding for the CRUK/MRC Oxford Institute for Radiation Oncology.

Received: June 20, 2014; accepted: April 7, 2015; published online: June 29, 2015

REFERENCES

1. Watson SJ, Jones AL, Oatway WB, Hughes JS. Ionising radiation exposure of the UK population: 2005 Review HPA-RPD-001 Chilton: Health Protection Agency Radiation Protection Division; 2005.
2. Health effects of exposure to radon, BEIR VI. National Research Council, Washington DC: National Academy Press; 1999.
3. Elgqvist J, Frost S, Pouget JP, Albertsson P. The Potential and hurdles of targeted alpha therapy - clinical trials and beyond. Front Oncol 2014; 3:324.
4. Folkard M, Prise KM, Vojnovic B, Newman HC, Roper MJ, Michael BD. Inactivation of V79 cells by low-energy protons, deuterons and helium-3 ions. Int J Radiat Biol 1996; 69:729–38.
5. Friedrich T, Grun R, Scholz U, Elsasser T, Durante M, Scholz M. Sensitivity analysis of the relative biological effectiveness predicted by the local effect model. Phys Med Biol 2013; 58:6827–49.
6. Brahme A. Accurate description of the cell survival and biological effect at low and high doses and LET's. J Radiat Res 2011; 52:389–407.
7. Stewart RD, Yu VK, Georgakilas AG, Koumenis C, Park JH, Carlson DJ. Effects of radiation quality and oxygen on clustered DNA lesions and cell death. Radiat Res 2011; 176:587–602.
8. Task Group on Radiation Quality Effects in Radiological Protection, Committee 1 on Radiation Effects, Relative biological effectiveness (RBE), quality factor (Q), and radiation weighting factor (w(R)). International Commission on Radiological Protection. Ann ICRP 2003; 33:1–117.
9. Barendsen GW. Impairment of the proliferative capacity of human cells in culture by alpha-particles with differing linear-energy transfer. Int J Radiat Biol 1964; 8:453–66.
10. Sorensen BS, Overgaard J, Bassler N. In vitro RBE-LET dependence for multiple particle types. Acta Oncol 2011; 50:757–62.
11. Thacker J, Stretch A, Stephens MA. Mutation and inactivation of cultured mammalian cells exposed to beams of accelerated heavy ions. II. Chinese hamster V79 cells. Int J Radiat Biol 1979; 36:137–48.
12. Cox R, Masson WK. Mutation and inactivation of cultured mammalian cells exposed to beams of accelerated heavy ions. III. Human diploid fibroblasts. Int J Radiat Biol 1979; 36:149–60.
13. Miller RC, Marino SA, Brenner DJ, Martin SG, Richards M, Randers-Pehrson G, et al. The biological effectiveness of radon-progeny alpha particles. II. Oncogenic transformation as a function of linear energy transfer. Radiat Res 1995; 142:54–60.
14. Goodhead DT, Belli M, Mill AJ, Bance DA, Allen LA, Hall SC, et al. Direct comparison between protons and alpha-particles of the same LET: I. Irradiation methods and inactivation of asynchronous V79, HeLa and C3H 10T1/2 cells. Int J Radiat Biol 1992; 61:611–24.
15. Goodhead DT, Bance DA, Stretch A, Wilkinson RE. A versatile plutonium-238 irradiator for radiobiological studies with alpha-particles. Int J Radiat Biol 1991; 59:195–210.
16. Goodhead DT, Thacker J. Inactivation and mutation of cultured mammalian cells by aluminium characteristic ultrasoft X-rays. I. Properties of aluminium X-rays and preliminary experiments with Chinese hamster cells. Int J Radiat Biol 1977; 31:541–59.
17. Botchway SW, Stevens DL, Hill MA, Jenner TJ, O'Neill P. Induction and rejoining of DNA double-strand breaks in Chinese hamster V79-4 cells irradiated with characteristic aluminum K and copper L ultrasoft X rays. Radiat Res 1997; 148:317–24.
18. Townsend KM, Stretch A, Stevens DL, Goodhead DT. Thickness measurements on V79-4 cells: a comparison between laser scanning confocal microscopy and electron microscopy. Int J Radiat Biol 1990; 58:499–508.
19. Hill MA, Stevens DL, Stuart Townsend KM, Goodhead DT. Comments on the recently reported low biological effectiveness of ultrasoft X rays. Radiat Res 2001; 155:503–10.
20. Townsend KM, Marsden SJ. Nuclear area measurement on viable cells, using confocal microscopy. Int J Radiat Biol 1992; 61:549–51.
21. Hill MA, Stevens DL, Bance DA, Goodhead DT. Biological effectiveness of isolated short electron tracks: V79-4 cell inactivation following low dose-rate irradiation with Al(K) ultrasoft X-rays. Int J Radiat Biol 2002; 78:967–79.
22. Ziegler JF. Helium stopping powers and ranges in all elemental matter. New York: Pergamon; 1977.
23. Ziegler JF, Biersack JP, Ziegler MD. SRIM The stopping and range of ions in matter. Chester, Maryland: SRIM Co.; 2008.
24. Hill MA, Herdman MT, Stevens DL, Jones NJ, Thacker J, Goodhead DT. Relative sensitivities of repair-deficient mammalian cells for clonogenic survival after alpha-particle irradiation. Radiat Res 2004; 162:667–76.
25. Cox R, Thacker J, Goodhead DT. Inactivation and mutation of cultured mammalian cells by aluminium characteristic ultrasoft X-rays. II. Dose-responses of Chinese hamster and human diploid cells to aluminium X-rays and radiations of different LET. Int J Radiat Biol 1977; 31:561–76.
26. Munson RJ, Bance DA, Stretch A, Goodhead DT. Mutation and inactivation of cultured mammalian cells exposed to beams of accelerated heavy ions. I. Irradiation facilities and methods. Int J Radiat Biol 1979; 36:127–36.

27. Goodhead DT. Relationship of microdosimetric techniques to applications in biological systems. In: Kase KR, Bjarngaard BE, Attix FH, editors. The dosimetry of ionizing radiation. Orlando: Academic Press; 1987. p. 1–89.
28. Goodhead DT, Munson RJ, Thacker J, Cox R. Mutation and inactivation of cultured mammalian cells exposed to beams of accelerated heavy ions. IV. Biophysical interpretation. Int J Radiat Biol 1980; 37:135–67.
29. Jenner TJ, Delara CM, O'Neill P, Stevens DL. Induction and rejoining of DNA double-strand breaks in V79-4 mammalian cells following gamma-irradiation and alpha-irradiation. Int J Radiat Biol 1993; 64:265–73.
30. Jenner TJ, Delara CM, Stevens DL, Burns NA, O'Neill P. The induction of DNA double-strand breaks in V79-4 cells by gamma and alpha radiations - complexity of damage. Radiat Prot Dosimetry 1994; 52:289–93.
31. Friedrich T, Scholz U, Elsasser T, Durante M, Scholz M. Systematic analysis of RBE and related quantities using a database of cell survival experiments with ion beam irradiation. J Radiat Res 2013; 54:494–514.
32. Furusawa Y, Fukutsu K, Aoki M, Itsukaichi H, Eguchi-Kasai K, Ohara H, et al. Inactivation of aerobic and hypoxic cells from three different cell lines by accelerated (3)He-, (12)C- and (20)Ne-ion beams. Radiat Res 2000; 154:485–96.
33. Barendsen GW, Walter HM, Fowler JF, Bewley DK. Effects of different ionizing radiations on human cells in tissue culture. III. Experiments with cyclotron-accelerated alpha-particles and deuterons. Radiat Res 1963; 18:106–19.
34. Nikjoo H, O'Neill P, Wilson WE, Goodhead DT. Computational approach for determining the spectrum of DNA damage induced by ionizing radiation. Radiat Res 2001; 156:577–83.
35. Cox R. A cellular description of the repair defect in ataxia-telangiectasia. In: Bridges BA, Harnden DG, editors. Ataxia telangiectasia: a cellular and molecular link between cancer, neuropathology, and immune deficiency. London: John Wiley and Sons; 1982. p. 141–53.
36. Griffiths SD, Marsden SJ, Wright EG, Greaves MF, Goodhead DT. Lethality and mutagenesis of B lymphocyte progenitor cells following exposure to alpha-particles and X-rays. Int J Radiat Biol 1994; 66:197–205.
37. Goodhead DT. Mechanisms for the biological effectiveness of high-LET radiations. J Radiat Res 1999; 40 Suppl:1–13.
38. Goodhead DT. Initial events in the cellular effects of ionizing radiations: clustered damage in DNA. Int J Radiat Biol 1994; 65:7–17.
39. Ward JF. The complexity of DNA damage: relevance to biological consequences. Int J Radiat Biol 1994; 66:427–32.
40. Nikjoo H, Bolton CE, Watanabe R, Terrissol M, O'Neill P, Goodhead DT. Modelling of DNA damage induced by energetic electrons (100 eV to 100 keV). Radiat Prot Dosim 2002; 99:77–80.
41. Goodhead DT. Energy deposition stochastics and track structure: what about the target? Radiat Prot Dosim 2006; 122:3–15.
42. deLara CM, Jenner TJ, Townsend KM, Marsden SJ, O'Neill P. The effect of dimethyl sulfoxide on the induction of DNA double-strand breaks in V79-4 mammalian cells by alpha particles. Radiat Res 1995; 144:43–9.
43. Rydberg B, Holley WR, Mian IS, Chatterjee A. Chromatin conformation in living cells: Support for a zig-zag model of the 30 nm chromatin fiber. J Mol Biol 1998; 284:71–84.
44. Lobrich M, Cooper PK, Rydberg B. Non-random distribution of DNA double-strand breaks induced by particle irradiation. Int J Radiat Biol 1996; 70:493–503.
45. Friedland W, Paretzke HG, Ballarini F, Ottolenghi A, Kreth G, Cremer C. First steps towards systems radiation biology studies concerned with DNA and chromosome structure within living cells. Radiat Environ Biophys 2008; 47:49–61.
46. Alloni D, Campa A, Friedland W, Mariotti L, Ottolenghi A. Track structure, radiation quality and initial radiobiological events: considerations based on the PARTRAC code experience. Int J Radiat Biol 2012; 88:77–86.
47. Belli M, Cherubini R, Dalla Vecchia M, Dini V, Esposito G, Moschini G, et al. DNA fragmentation in V79 cells irradiated with light ions as measured by pulsed-field gel electrophoresis. I. Experimental results. Int J Radiat Biol 2002; 78:475–82.
48. Newman HC, Prise KM, Michael BD. The role of higher-order chromatin structure in the yield and distribution of DNA double-strand breaks in cells irradiated with X-rays or alpha-particles. Int J Radiat Biol 2000; 76:1085–93.
49. Cremer T, Cremer C. Chromosome territories, nuclear architecture and gene regulation in mammalian cells. Nat Rev Genet 2001; 2:292–301.
50. Cremer M, von Hase J, Volm T, Brero A, Kreth G, Walter J, et al. Non-random radial higher-order chromatin arrangements in nuclei of diploid human cells. Chromosome Res 2001; 9:541–67.
51. Foster HA, Estrada-Girona G, Themis M, Garimberti E, Hill MA, Bridger JM, et al. Relative proximity of chromosome territories influences chromosome exchange partners in radiation-induced chromosome rearrangements in primary human bronchial epithelial cells. Mutat Res 2013; 756:66–77.
52. Paretzke HG. Radiation track theory. In: Freeman GR, editor. Kinetics of nonhomologous processes. New York: Wiley; 1987. p. 189.
53. Jakob B, Splinter J, Durante M, Taucher-Schoiz G. Live cell microscopy analysis of radiation-induced DNA double-strand break motion. Proc Natl Acad Sci U S A 2009; 106:3172–7.
54. Soutoglou E, Dorn JF, Sengupta K, Jasin M, Nussenzweig A, Ried T, et al. Positional stability of single double-strand breaks in mammalian cells. Nat Cell Biol 2007; 9:675–82.
55. Anderson RM, Stevens DL, Goodhead DT. M-FISH analysis shows that complex chromosome aberrations induced by alpha-particle tracks are cumulative products of localized rearrangements. Proc Natl Acad Sci U S A 2002; 99:12167–72.
56. Anderson RM, Papworth DG, Stevens DL, Sumption ND, Goodhead DT. Increased complexity of radiation-induced chromosome aberrations consistent with a mechanism of sequential formation. Cytogenet Genome Res 2006; 112:35–44.
57. Anderson RM, Stevens DL, Sumption ND, Townsend KM, Goodhead DT, Hill MA. Effect of linear energy transfer (LET) on the complexity of alpha-particle-induced chromosome aberrations in human CD34+ cells. Radiat Res 2007; 167:541–50.
58. Curwen GB, Tawn EJ, Cadwell KK, Guyatt L, Thompson J, Hill MA. mFISH analysis of chromosome aberrations induced in vitro by alpha-particle radiation: examination of dose-response relationships. Radiat Res 2012; 178:414–24.
59. Durante M, Pignalosa D, Jansen JA, Walboomers XF, Ritter S. Influence of nuclear geometry on the formation of genetic rearrangements in human cells. Radiat Res 2010; 174:20–6.
60. Themis M, Garimberti E, Hill MA, Anderson RM. Reduced chromosome aberration complexity in normal human bronchial epithelial cells exposed to low-LET gamma-rays and high-LET alpha-particles. Int J Radiat Biol 2013; 89:934–43.